High-Order Moment Models of Landmark Distribution for Local Homing Navigation

CHANGMIN LEE AND DAEEUN KIM

School of Electrical and Electronic Engineering, Yonsei University, Seoul 03722, South Korea

Corresponding author: Daeeun Kim (daeeun@yonsei.ac.kr)

ABSTRACT For local homing navigation, a mobile robot is supposed to return home using snapshots of the surrounding environment. It basically follows the snapshot model, comparing the home snapshot and the current view to determine the homing direction. In this paper, we suggest a high-order moment potential to describe the landmark feature distribution for local homing navigation. The moment potential function calculates the sum of products of the feature and the distance of landmark particles as a holistic view, allowing a high order of the distance. It effectively combines the range sensor values of landmarks in the current view and the visual features. By analogy with the moment in physics, the center of the moment is estimated as the reference point, which is the unique convergence point in the convex moment potential from any view, and using the property, the gradient of moment potential at the current position and home location can derive the homing vector. We provide a proof of convergence for any moment potential with order greater than or equal to one. Also, we demonstrate homing performances with various moment models in real environments to validate our models. The suggested moment models combining both landmark distance and visual feature have better performances than the visual information alone, and high-order moment potentials can be searched to obtain a better description of landmark distribution for a given environment.

INDEX TERMS Visual navigation, bio-inspired navigation, snapshot model, high-order moment function, convergence point, landmark distribution, sensor fusion.

I. INTRODUCTION

There have been many types of local navigation studies from wheeled vehicles to autonomous unmanned vehicles. Recently, for example, many robots are operated in the normal land with simple wheeled vehicles [1], aerial vehicles [2], underwater vehicles [3], and space robots [4]. They handle various sensors including vision [5], inertia sensor [6], RFID [7] and other sensors [8], [9]. Many navigation algorithms have been developed with those sensor readings and sensor-to-motor mappings.

Insect navigation has inspired many engineering models for navigation system. Insect navigation is often based on odometry and vision information. Path integration with odometry has been suggested [10]–[14], and it accumulates internal signals for the movements of the insect and calculates homing direction. However, this model can have cumulative errors from internal measurements. There have been studies to support visual cues for insect navigation [15]–[17]; the skyline, the sun or moon's location, the polarized pattern of lights affect navigation. Also, it is well-known that vision is a common tool in navigation for many species including gerbils, jellyfish, rodents and fiddler crab [18]–[20], while olfactory, auditory, odometry, magnetic senses can be another cues to help navigation [21]–[23]. It was argued that the ant uses visual cues in early trajectories building path integration [14]. Similar results were also observed in various species including bees [24], wasp [25] and dung beetle [25].

In this paper, we mainly use a bio-inspired navigation method called snapshot model [26]. The snapshot model originates from the bee navigation model. It uses only two snapshot images at the home location and the current location. The homing direction can be determined by the direction reducing the difference between the two images. The snapshot model as a bio-inspired model has induced many variations for engineering applications. The bio-inspired model can be largely classified into three categories, the parameter-based approach, the pixel-based approach and the warping method.

The parameter-based approach uses relative location or angular position of landmarks. The Average Landmark Vector (ALV) model [27] uses unit length vectors pointing landmarks with no distance information. The sum of these

unit vectors is called the average landmark vector for a given snapshot. The snapshot model compares two ALVs for snapshots observed at the home location and the current location, to determine the homing direction. The model has been used in many robotic applications. As an extension of the work, the Distance Estimated Landmark Vector (DELV) model allows the distance to landmarks [28], [29]. Also, feature extractions and the ALV model have been combined to improve the homing navigation [30], [31]. That is, the method extracts, for example, SIFT features over two snapshot images and determines the homing direction. Another method used optical flows to detect the motion pattern of feature points, caused by the relative motion of an observer [32]. Visual navigation is often involved with feature extraction process [31], [33]. Identifying appropriate feature points for snapshots can help estimate the movement direction or distance between a pair of snapshots. However, it may require complex computing process.

Another approach as a pixel-based approach is the Descent in Image Distance (DID) method, which estimates the relative distance depending on the image difference. The primitive model of DID [34] decides homing direction by taking snapshots in the surrounding locations about the current spot and finding the one with the smallest difference from the home snapshot image. Advanced DID models [35], [36] use the difference ratio between each candidate image and the home image. Furthermore, they applied the matched filter to estimate the candidate images without additional movements. The visual compass method using the image difference concept is useful to find the alignment (relative orientation) for two snapshots, when there is no reference compass available [34]. The approach can be extended into a view-based method [37]. The snapshot matching algorithm with optic flow has been applied to the aircraft finding the current location using snapshot images [38]. Another method using scale space [39] uses correspon- dences with SIFT features to calculate optical flows and also an orientation invariant visual homing has been suggested [40].

The third category method as a bio-inspired model is the warping method which handles possible matching parameters for comparison of two snapshot images. The 1D-warping model [41]–[43] considers predicted images depending on the parameters from the egocentric view, such as orientation angle and view angle to landmarks. The best-matching snapshot with the home image can estimate the homing direction. Furthermore, 2D-warping model and min-warping model [44]–[46] consider more environmental parameters as an extension of the warping idea. The warping model is a pixel matching approach and it needs no feature extraction process. It thus provides robust robotic application. The min-warping is an advanced model to demonstrate success in real applications [47]–[49]. Also, warping methods with various features including SURF and SIFT have been tested for robotic experiments [50], [51]. Warping with optical flow has been tested [52], and the min-warping with particle filter has been used to localize the cleaning robot in the

environmental map. The warping-based approaches have robustness even under various illumination conditions [49], [53]. However, the warping approach considers all the environmental parameters to influence the snapshot image and needs high computing time.

Recently, the snapshot model with range sensor has been tested [29], [54], which is effective in homing performance and even in the alignment of orientation of two snapshots. The moment model has been used in physics to consider the mass distribution. The moment concept has been applied to the navigation system [55]. Previously, we investigated the model similar to the second moment of inertia to represent landmark distribution, where the range sensor and color intensity can be combined together in the moment model [56]. In this paper, we suggest high-order moment models as an extension of the previous work, and provide a proof that local homing navigation is successful to reach the goal, starting at any position, when it is assumed that the moment measure holds constant from any view. It follows the snapshot model and a holistic approach with the whole pixel information is applied to build the moment potential. Various forms of moment models with range information and color intensity will be tested. We apply a concept of various moment functions to our new navigation model based on holistic matching of snapshot images.

Here, we seek to answer the following questions: Is the order of moment model important to improve the homing performance? How can we determine homing vectors with high-order moment models? Under what conditions can local homing navigation reach the goal from any starting position? Is the distance information of landmarks a cruicial factor in the moment model? Can the model estimate the moment potential even without range sensor?

II. METHODS
A. EXPERIMENTAL ENVIRONMENT
A mobile robot with two wheels (Roomba, Create 4400, iRobot, Bedford, MA, USA) was used to test local homing navigation. The robot is mounted with an omnidirectional camera (Logitech Webcam E3500 vision sensor with a sphere-shaped mirror) and a range sensor (URG-04LX-UG01, HOKUYO, Osaka, Japan). The two different sensors can read the environmental information at an arbitrary position. A labtop computer is connected with those sensors and also the mobile robot via USB serial ports. It runs MATLAB 2017a software to test a control program.

The robot is positioned in an indoor environment with many landmarks, a classroom arena, about 6 meter by 6 meter, including a desk, drawers, trash cans, large vases, windows and walls – see Fig. 1. The omnidirectional camera takes a snapshot which can be converted into a panoramic image with a resolution of 0.5 degree. The laser sensor can cover 240 degrees with a resolution of 0.36 degree. Two overlapped shots can make omnidirectional range data, which is converted into 720 samples in a panoramic range. As a result, the range data has the same resolution with the visual panoramic image. Each pixel along the horizontal line in the panoramic
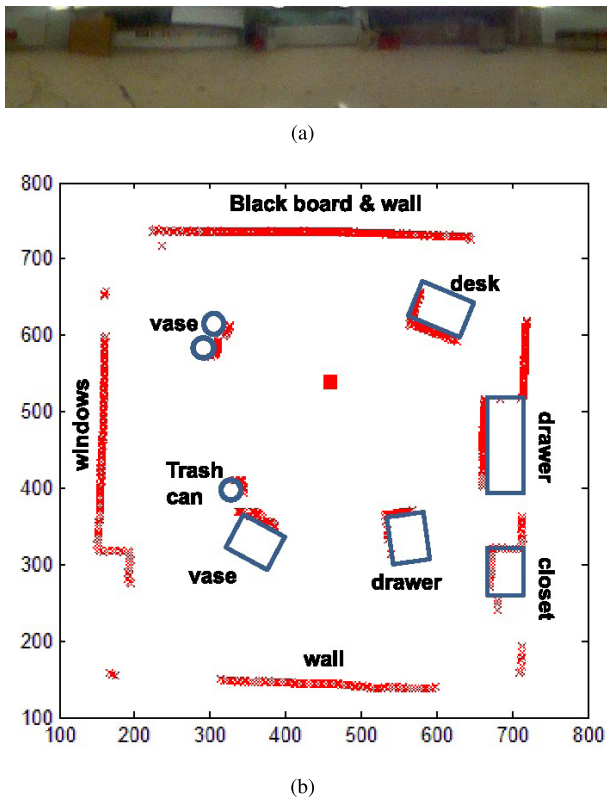
(a)

(b)

FIGURE 1. Visual image and laser sensor readings for an environment called 'ourlab' (a) panoramic image converted from an omnidirectional image (b) range data map (red square indicates the capturing position and x marks show the distance map).

snapshot can match one by one with a sample in the range data. Fig. 1 shows an example of panoramic image and range data for the surrounding environment. It builds a reference map consisting of depth information for landmarks and color intensity.

B. MOMENT MODEL
The physical model of moment evaluates a mass distribution as a quantitative measure of the shape of points. By analogy, the moment is defined as a distribution of points in the navigation model. For a given set of landmarks in the environment, the landmark distribution can be represented as a combination of their positions and features. The height, color intensity or visual features of landmarks can be feature candidates. A landmark can be an object identified from the background, or a pixel in the image plane without object feature extraction. In the snapshot image, the color pixels in the omnidirectional view can be landmarks with the color intensity and the range information.

We define a moment function M_n as follows:

$$M_n = \sum_{i=1}^{N} M_{i,n} = \sum_{i=1}^{N} r_i^n C_i$$

$$= \sum_{i=1}^{N} ((a_i - x)^2 + (b_i - y)^2)^{\frac{n}{2}} C_i \quad (1)$$
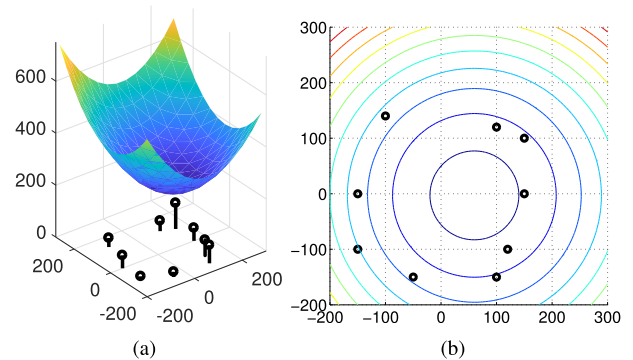

(a)

(b)

FIGURE 2. An example of moment potential (a) convex shape of moment potential where each landmark has its own height and the height is used as a feature value (b) contour for equi-potential lines; the center of circles indicates the point with the minimum potential.

where n is the moment order, r_i is the i-th range value from the observing point, C_i is the i-th feature value, N is the number of samples (measurements), (a_i, b_i) is the location for the measured feature, and (x, y) is an arbitrary position of the robot measuring the moment potential. The order n determines the moment characteristics, and especially the moment function with order $n = 2$ is similar to the second moment of inertia in physics.

We take the moment measure as a potential function and an interesting property with the moment is that it has the global minimum point for order $n \geq 1$. We provide a proof for the convex property with the moment function – see Appendix. Fig. 2 shows an example of moment potential with order $n = 2$, where a set of landmarks are distributed in an arena and each landmark has varying height. We observe that the unique convergence point to the minimum potential is available at (80,0).

We calculate the gradient of the moment function as follows:

$$\nabla M_n = \sum_{i=1}^{N} n r_i^{n-2} \ [(x - a_i)C_i, \ (y - b_i)C_i] \quad (2)$$

where (x, y) is a position to measure the moment potential. A collection of features C_i, for $i = 1, ..., N$ are observed at the relative position (a_i, b_i) from an observing point P. We assume that the features are commonly observed at any position and their relative position (a_i, b_i) can change depending on the observing point. The relative coordinates are measured from the current position or the observing point. With the relative coordinate, we try to find the location with the minimum moment potential by setting the gradient to zero, since the potential function is convex.

If the order n is equal to 2, we can easily find the convergence point with the global minimum potential by $\nabla M_n = 0$ in equation (2) as given by

$$(X_c, Y_c) = \left(\frac{\sum_{i=1}^{N} a_i C_i}{\sum_{i=1}^{N} C_i}, \quad \frac{\sum_{i=1}^{N} b_i C_i}{\sum_{i=1}^{N} C_i} \right) \quad (3)$$

For high-order n, we know there is a unique minimum moment value, but it is not easy to calculate the accurate convergence point at once, satisfying the equation

$$\sum_{i=1}^{N} n\{(a_i - X_c)^2 + (b_i - Y_c)^2\}^{n/2-1} \times (X_c - a_i)C_i = 0$$

$$\sum_{i=1}^{N} n\{(a_i - X_c)^2 + (b_i - Y_c)^2\}^{n/2-1} \times (Y_c - b_i)C_i = 0 \quad (4)$$

Let $R_c = (X_c, Y_c)$ be the convergence point in the coordinate measured from the current position P. Similarly, another collection of features C_i' at the relative position (a_i', b_i') from the home location can be observed and then a new convergence point $R_h = (X_h, Y_h)$ satisfying the equation (4) is available in the coordinate of the home location $\bar{H}$, It is assumed that the same landmark features are observed at any position, and the series C_i for $i = 1, .., N$ should have the same pattern with C_i'.

Hence, the homing vector $\overrightarrow{H}$ can be estimated by

$$\overrightarrow{H} = \bar{H} - C \simeq R_c - R_h \quad (5)$$

where R_c, R_h are the reference points (convergence points) in the coordinate of the current position and the home position, respectively and then we can take $C + R_c = \bar{H} + R_h$. The position $C + R_c$ be the reference point using the current view in the absolute coordinate and we assume that it is the same as the point $\bar{H} + R_h$ using the home view.

Each observing point has its own coordinate but there exists a unique convergence point which is the same location in the absolute coordinate, regardless of any relative coordinate. (a little deviation of the convergence point may be observed due to landmark occlusions or noisy sensor readings on the distance or the feature value). By the fact that the moment potential function has a convex shape, the global minimum potential can be reached or estimated from any observing point. To estimate the homing vector, we need a condition that the environment is isotropic, that is, all landmarks and their features are commonly observed at any position.

We apply the numerical method based on the iterative gradient descent search for the convergence points.

$$(X_{t+1}, Y_{t+1}) = (X_t, Y_t) - \gamma_t \nabla M_n((X_t, Y_t)) \quad (6)$$

$$\gamma_t = \frac{D_t[\nabla M_n(X_t, Y_t) - \nabla M_n(X_{t-1}, Y_{t-1})]^T}{||\nabla M_n(X_t, Y_t) - \nabla M_n(X_{t-1}, Y_{t-1})||^2} \quad (7)$$

$$D_t = (X_t - X_{t-1}, \ Y_t - Y_{t-1}), \quad (8)$$

where (X_t, Y_t) is the updated location for the convergence point in step t and γ_t is a learning rate in the gradient descent. It is terminated when the amount of change for each step is smaller than 0.1.

To reduce the computing time to find the location of convergence points, we can use a gradient-descent method to sketch roughly the homing vector.

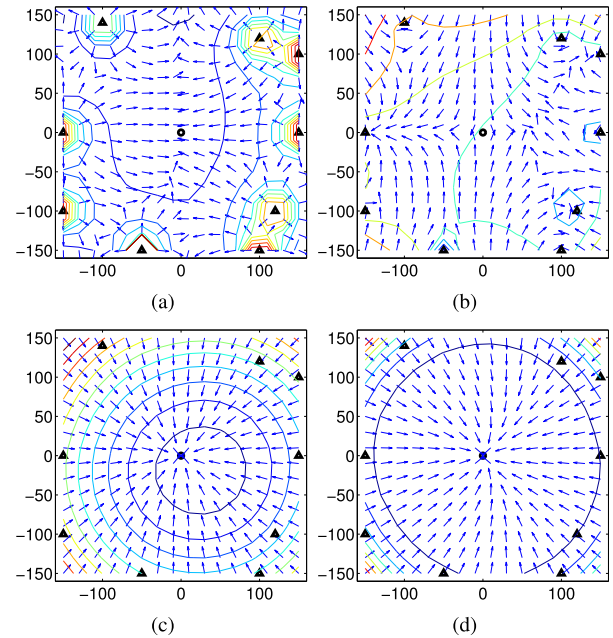$$\overrightarrow{H}(x, y) = \eta(\nabla M_n^H - \nabla M_n^C) \quad (9)$$

FIGURE 3. Simulation environment and homing vectors with various moment functions; vector maps for the order $n = -1, 0.2, 2, 10$ (curved lines show the contour lines of moment potential, black dot indicates the home location, and triangles show the location of landmarks). (a) $n = -1$. (b) $n = 0.2$. (c) $n = 2$. (d) $n = 10$.

where η is a scaling parameter, ∇M_n^H, ∇M_n^C are gradients of moment potential at the home location and the current position, respectively, and $\overrightarrow{H}_n(x, y)$ is the estimated homing vector at the current location (x, y). We apply $(x, y) = (0, 0)$ in equation (2) to estimate the gradients at the current position and at the home position, respectively. The relative distances for the corresponding features are changed depending on the observing point. Estimating the homing direction is not influenced by the scaling parameter η. We will mainly use the above formulation for later experiments to evaluate the homing direction at an arbitrary position.

In a simulation environment with a set of landmarks including height information, we can test the above convergence property. Fig. 3 shows the estimated homing vectors with varying moment orders. With $n = -1$, arrows show directions away from objects and the vectors have collision avoidance property. The order $n = 0.2$ has a failure in the convergence in the contour map. For the other two cases with $n > 1$, there is a unique point with the minimum potential and thus they can have desired homing vectors.

C. AREA MOMENT MODEL

With the above moment function, we can assume that an object is a landmark, or an object consists of landmark particles. If we use the range sensor and vision sensor, the information of distance and the pixels on the horizontal line can be collected. Each pixel in the outer boundary can be treated as a landmark, and 720 pixels along the horizontal line in the panoramic snapshot become a whole set of landmarks.
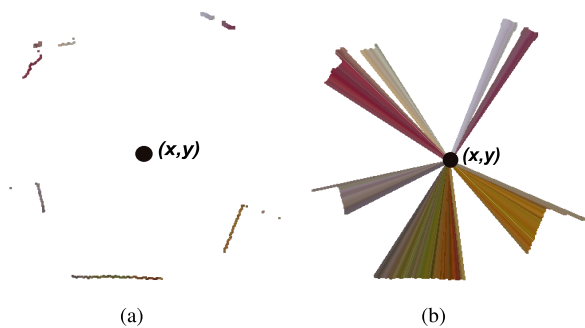
(a)   (b)

FIGURE 4. Two types of moment models (a) perimeter (landmark position) integration for the outer boundary (b) area integration.

As observed in the physical moment model, we can integrate the area covered with a given feature, assuming that the area is filled with the feature, like the area moment of inertia in physics. Fig. 4 shows two types of moment models, the perimeter integration and the area integration. The previous moment function shown in equation (1) follows the perimeter integration model. The moment function for the area integration is changed as follows:

$$M_n = \int_0^{2\pi} \int_0^{r_\theta} r^n C_\theta \rho \, dA \, d\theta = \int_0^{2\pi} C_\theta \int_0^{r_\theta} r^n \rho (r \, dr \, d\theta) \tag{10}$$

where M_n is the area moment level, r is the distance to a feature, C_θ is the feature uniformly distributed over each angular direction, and ρ is the density of the feature.

The equation can be re-written as

$$M_n = \rho \int_0^{2\pi} C_\theta \int_0^{r_\theta} r^{n+1} \, dr \, d\theta \tag{11}$$

$$= \rho \int_0^{2\pi} \frac{1}{n+2} r_\theta^{n+2} C_\theta \, d\theta \tag{12}$$

$$\cong \alpha \sum_{i=1}^N r_i^{n+2} C_i \tag{13}$$

where N is the number of landmarks, r_i is the distance to the i-th feature, and α is the scaling parameter. To estimate the moment potential for a given environment, a discretized moment function given in equation (13) can be applied, and it shows the order n is only increased to $n + 2$ for the area moment. For robotic experiments, we will take only the perimeter integration.

D. COMPARISON OF MOMENT MODELS

The high-order moment model that we suggest is based on the landmark distance and the feature. Many combinations of choices on the distance, the feature and the moment order are available in the moment function. There are options of what features can be selected in the moment model, what order of the moment function will be used, whether the range sensor is available or the distance can be estimated with the ground line in the visual image, or what kind of alignment methods will

be used – see Table 1. Each class name follows the feature characteristics, distance estimation type and the alignment method; for example, elc(n) indicates Equal intensity for the feature ($C_i = 1$), Laser sensor readings for landmark distances and Compass for the alignment.

In the moment model, we can select the color intensity as the feature C_i. To see the effect of the color intensity, we test together the equal intensity $C_i = 1$ for every landmark. The distance r_i in the moment function can be obtained with a laser sensor or the ground line estimation in the visual image. The ground line is the border line between the floor ground and a landmark object, which contrasts the color intensity in a given angular direction and can be detected easily in the visual image. The landmark distance can be roughly estimated in proportion with the number of pixels up to the ground line from the bottom of the panoramic image. In contrast, the laser sensor reads the distance information directly with its measurement. The moment function has order $n \geq 1$ for its convex property, and we test varying n's to see the effect of order n.

The moment-based methods that we suggest follow the snapshot model in which a pair of snapshots at the current location and at the home location are compared to determine the homing direction. With a reference compass, two snapshots can be aligned for the orientation. However, an alignment algorithm is needed to match the orientation for a pair of snapshots in the application without a reference compass. Here, we will test two alignment methods for the orientation, visual compass [34] and landmark rearrangement method [57].

With the visual compass method [34], the home snapshot is taken as a reference image, and the current view is rotated by a unit angle until the rotated view image and the home image have the minimum image difference. The matched angle is the orientation angle of the current view to align with the reference image. Another alignment method called landmark rearrangement [57] is tested. A set of landmarks observed in the home coordinate should one by one correspond to another set of landmarks observed at the current position, since we assume that the environment is isotropic in the snapshot model. Similar to the visual compass, the current view is rotated to match the home snapshot but a set of landmark vectors in the current view are re-mapped in the opposite direction with landmarks observed in the reference image. If the two snapshots are aligned well, the sum of the resulting vectors will have end points most likely converging to a point with small variance. Otherwise, the end points have a distribution with a large variance. The variance is a criterion to determine the orientation angle of the current view relative to the reference image.

In this paper, we test high-order moment models of landmark distribution and features. The moment models will be compared with the conventional algorithm called DID for homing navigation. The Descent In image Distance (DID) model [34] uses three reference images. The original DID model finds homing direction by comparing images at the

TABLE 1. Methods classified by the feature, the range sensor and the alignment process (*n* is the moment order).

class	method	feature	range	alignment
elc(n)	moment	equal intensity	laser sensor reading	aligned by compass
egc(n)	moment	equal intensity	ground-line distance	aligned by compass
clc(n)	moment	color intensity	laser sensor reading	aligned by compass
cgc(n)	moment	color intensity	ground-line distance	aligned by compass
cec	moment	color intensity	equal distance	aligned by compass
did-c	DID	color intensity	image distance	aligned by compass
elv(n)	moment	equal intensity	laser sensor reading	visual compass
egv(n)	moment	equal intensity	ground-line distance	visual compass
clv(n)	moment	color intensity	laser sensor reading	visual compass
cgv(n)	moment	color intensity	ground-line distance	visual compass
elr(n)	moment	equal intensity	laser sensor reading	landmark rearrangement
egr(n)	moment	equal intensity	ground-line distance	landmark rearrangement
clr(n)	moment	color intensity	laser sensor reading	landmark rearrangement
cgr(n)	moment	color intensity	ground-line distance	landmark rearrangement
did-v	DID	color intensity	image distance	visual compass

surrounding positions of the current spot with the home snapshot. It needs an effort to collect snapshot images around the current position. In our experiments, two snapshots near the home location (taken at the positions moved in the orthogonal direction from the home location) and the home snapshot are compared with the snapshot taken at the current location. The method compares three pairs of snapshots to calculate the image distances. The relative image difference between each pair of snapshots can determine the homing direction.

Table 1 shows various methods with the moment model. With a reference compass, each method is classified depending on varying moment orders, two possible choices for the feature, color intensity or equal intensity, another two choices of the range, distance readings from laser sensor or distance estimation from the ground line in the image, Four possible cases in addition to the DID method are listed with a reference compass. Without a reference compass, two possible alignment methods, visual compass or landmark rearrangement are tested with color intensity as the feature.

III. EXPERIMENTAL RESULT

We evaluate the homing performance for various methods described above. The desired homing direction is the direction on the direct path from the current location to the target position (home location). From a pair of snapshots at the current location and the home location, we can determine the homing direction and compare it with the desired direction. The angular errors for homing can be measured for the performance evaluation. To validate the suggested high-order moment model, we tested two different indoor environments, 'ourlab' environment including several objects in an indoor office environment, which has 34 points for snapshots and laser sensor readings, and Vardy's dataset environment called 'a1original' [35]. Its area size is 2.7 m by 4.3 m and there are 170 grid points for the omnidirectional snapshots but no laser sensor data are available.

A. MOMENT MODELS WITH LASER SENSOR READINGS
Initially, we tested 'ourlab' environment shown in Fig. 1. The robot is surrounded by many objects. The omnidirectional
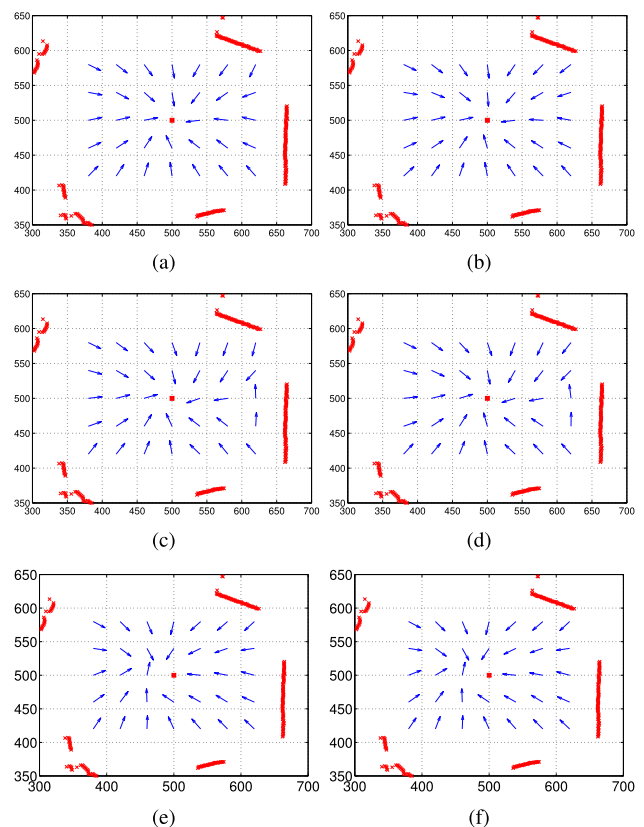

FIGURE 5. Homing experiments with laser sensor readings and color intensity for the feature; the first row indicates alignment by a reference compass, the second row alignment by visual compass, and the third row by landmark rearrangement. The columns show the order $n = 2$, and $n = 3$ in sequence, respectively. (red square at (500,500) indicates home and the arrow at each grid point shows the homing direction)

image has a set of landmark pixels as a holistic view, without any object feature extraction process. We determine the homing direction using equation (9) with sensor readings of range sensor and vision camera. Here, the color intensity for each pixel is a characteristic feature with distance information.

The moment function uses the distance information of landmarks and the landmark features. Fig. 5 shows the results
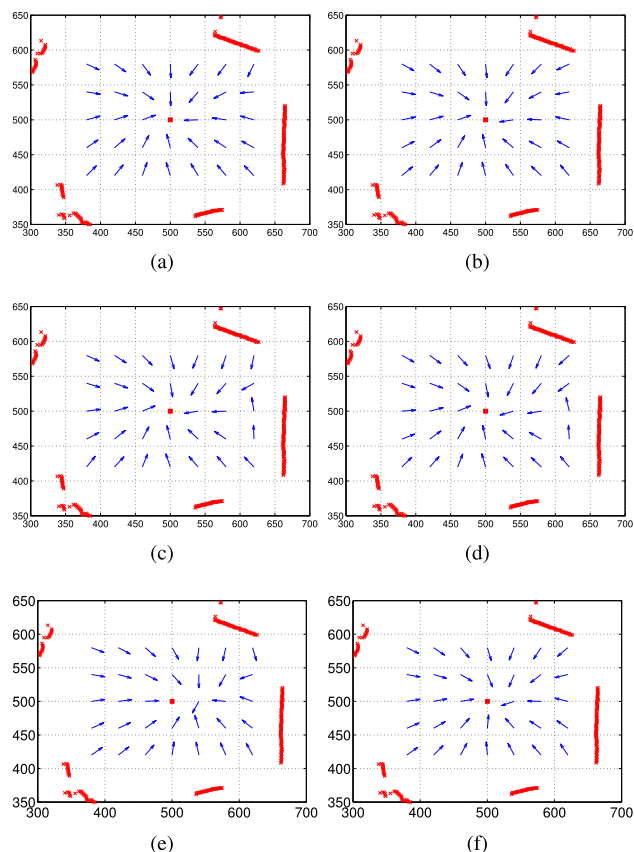
FIGURE 6. Homing experiments with laser sensor readings but equal intensity for the feature ($C_i = 1$); the first row indicates alignment by a reference compass, the second row alignment by visual compass, and the third row by landmark rearrangement. The columns show the order $n = 2$ and $n = 4$ in sequence, respectively. (red square at (500,500) indicates home and the arrow at each grid point shows the homing direction)

FIGURE 7. Homing experiments with estimated distance but equal intensity for the feature ($C_i = 1$); the first row indicates alignment by a reference compass, the second row alignment by visual compass, and the third row by landmark rearrangement. The columns show the order $n = 2$ and $n = 3$ in sequence, respectively. (red square at (500,500) indicates home and the arrow at each grid point shows the homing direction)

with varying moment orders and confirms the convergence proof that the homing vector based on the moment model converges into the home location. With a reference compass, the homing accuracy is much improved. Alignment by visual compass or landmark rearrangement mostly finds the right orientation of visual snapshots. Especially, the moment orders 2 and 3 have similar homing accuracy demonstrated.

We tested homing performance with an equal intensity for the feature ($C_i = 1$), but the range sensor used. Fig. 6 shows the results and the range sensor greatly contribute to the homing performance. Many angular errors are observed without a reference compass. The moment order slightly influences the performance. Surprisingly, we can see little effect of color intensity by comparing Fig. 5 and Fig. 6.

B. MOMENT MODELS WITH ESTIMATION OF GROUND-LINE DISTANCE

The moment models assume that the distance sensor is available. The feature and distance information are combined into the moment potential. Without a range sensor, the models may assume an equal distance of landmarks. Another way is to estimate the distance roughly with the ground-line of objects separated from the floor. Fig. 7 shows the results with
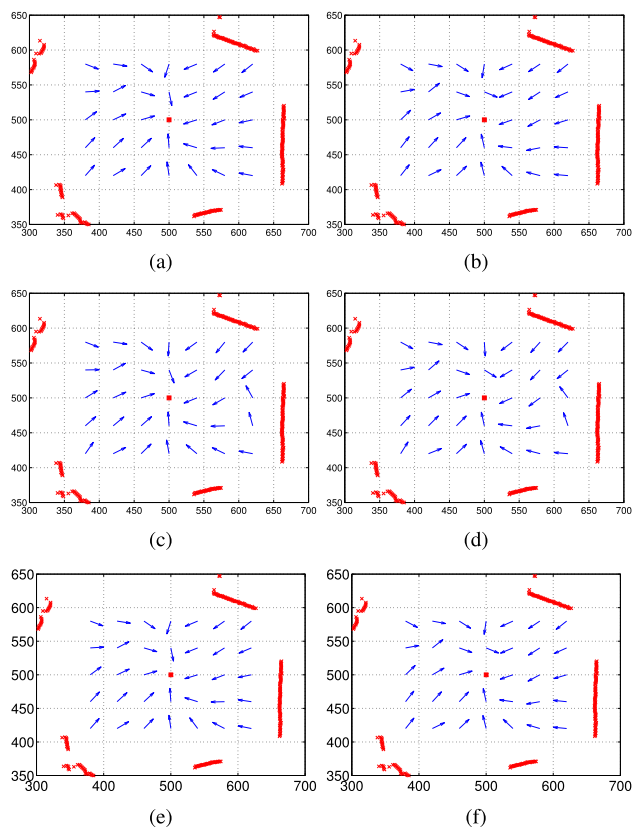
an equal intensity of landmark feature, which are comparable with the direct measurement of the distance. We will later see the effect of the distance measure in details.

We tested the ground-line distance to landmarks and color intensity for the landmark feature. Fig. 8 shows the results and the color intensity improves the homing performance in this case – see Fig. 7 and Fig. 8. Yet angular errors for homing are observed at several grid points. Direct measurement of landmark distance can further improve the homing performance, although the ground-line distance estimation mostly guides homing direction. When visual compass and landmark rearrangement are compared, alignment by landmark rearrangement has better peformance, regardless of the moment order.

Fig. 9 shows the result with varying moment orders for different landmark features and we observe that the order $n = 3$ or $n = 4$ shows the best average performance in the 'ourlab' environment. No discriminative landmark feature, that is, equal intensity for the feature, and the distance measured with laser sensor readings show similar results with landmarks including color-intensity features. It indirectly shows that the distance information is a major factor to influence the homing performance with the moment model.

We evaluated homing vectors with varying moment orders for Vardy's environment 'a1original'. In this environment,
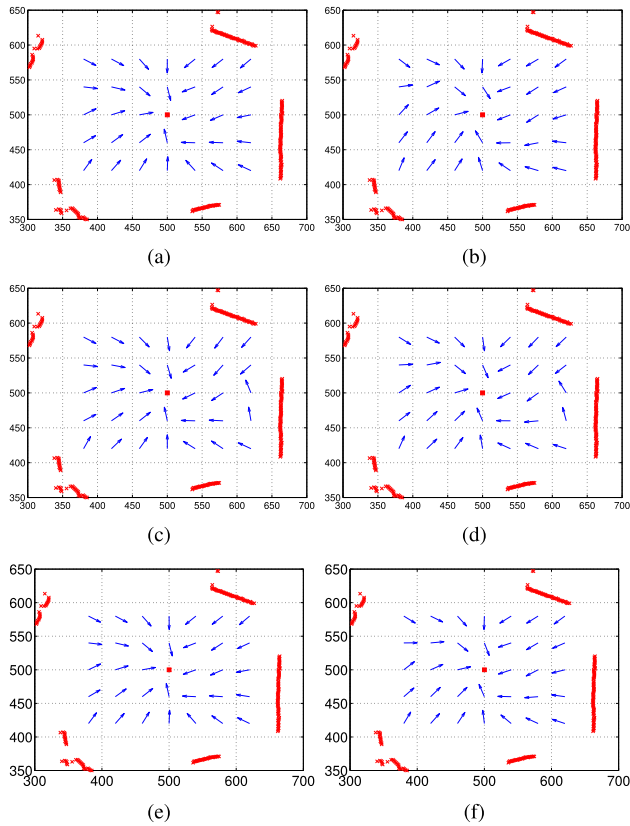
FIGURE 8. Homing experiments with estimated distance and color intensity for the feature; the first row indicates alignment by a reference compass, the second row alignment by visual compass, and the third row by landmark rearrangement. The columns show the order $n = 2$ and $n = 4$ in sequence, respectively. (red square at (500,500) indicates home and the arrow at each grid point shows the homing direction)
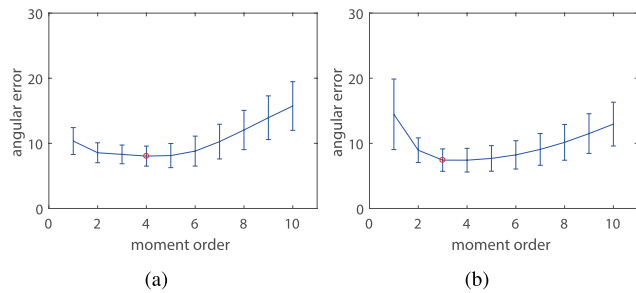

FIGURE 9. Homing performance with varying moment orders for 'ourlab' environment (with a reference compass and laser sensor readings); (a) equal intensity for landmark feature ($C_i = 1$) (b) color intensity (C_i: rgb color).

no range sensor data is available. We thus estimated the landmark distance with ground line in the image. Fig. 10-11 show the results for homing performance. The color intensity was applied for each point feature. Fig. 10 shows the angular errors depending on the moment order. The high-order moment models are effective for homing in this environment. The homing performance a little depends on the order. Increasing the order tends to produce more direct path to the home location although at most of grid points, they have similar homing patterns – see Fig. 11.
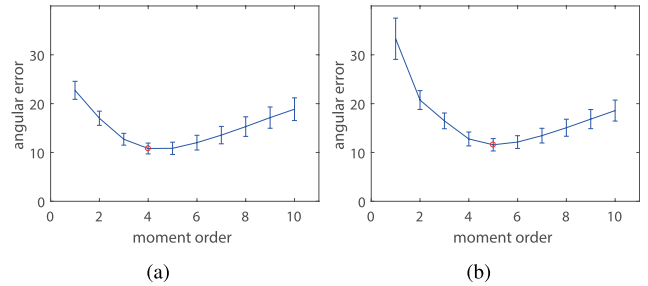

FIGURE 10. Homing performance with varying moment orders for Vardy's environment (a) equal intensity (b) color intensity for the feature (red dots indicate the minimum averaged error).
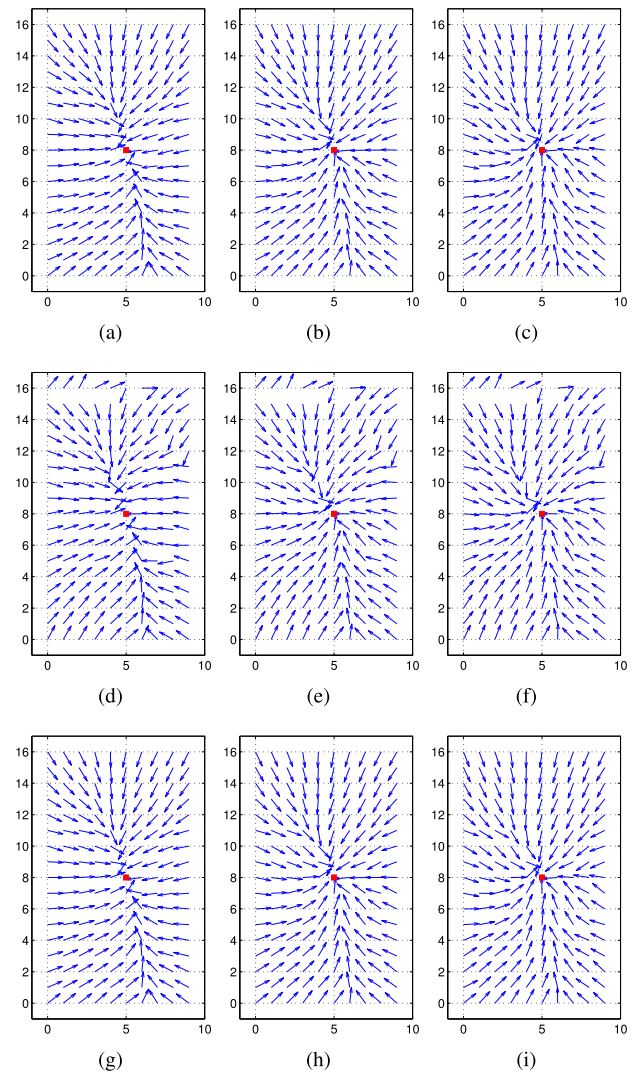

FIGURE 11. Homing experiments with estimated distance and color intensity for the feature in Vardy's environment; the first row indicates alignment by a reference compass, the second row alignment by visual compass, and the third row by landmark rearrangement. The columns show the order $n = 2$, $n = 4$, and $n = 5$ in sequence, respectively. (red square at (500,500) indicates home and the arrow at each grid point shows the homing direction)

The homing vector is largely influenced by what kind of alignment methods is applied. Without a reference compass, landmark rearrangement is better than visual compass
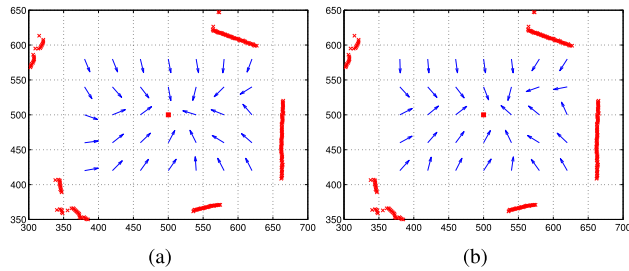
FIGURE 12. Homing performance with the DID method (a) aligned by a reference compass (b) aligned by visual compass (red square at (500,500) indicates home and the arrow at each grid point shows the homing direction).
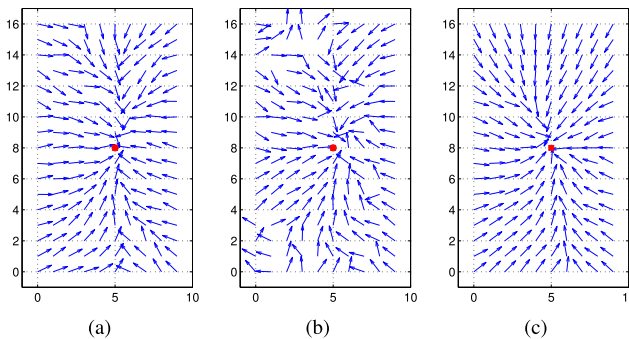

FIGURE 13. Homing experiments for Vardy's environment (a) DID with alignment by a reference compass (b) DID with alignment by visual compass (c) moment model with order $n = 4$ by landmark rearrangement using color information and ground-line distance (red square at (5,8) indicates home and the arrows show homing directions).

with the moment models. As shown in Fig. 10, the order $n = 4$ or 5 shows the minimum angular error. High-order moment function is useful to obtain good homing performance, but the order greater than 5 degrades the performance. It is due to the homing vector estimation based on the gradient-descent method in equation (9).

C. COMPARISON WITH THE DID METHOD

The moment potential uses laser sensor readings and visual sensing. Vision-based homing has been suggested and the DID (Descent in Image Distance) method estimates the relative distance between snapshot-capturing points to determine homing direction. Fig. 12 shows the results with the DID method for ourlab environment as the conventional algorithm. With a reference compass or visual compass, the method shows reasonable homing performance, but it is worse than the moment models in the homing accuracy at many grid points. The DID method uses only visual images without laser sensor readings, but allow three comparisons between the current view and home snapshots to calculate the image distance. From the results, it can be argued that the moment models are better than the DID method.

Similarly, we measured homing vectors with the DID method for Vardy's environment – see Fig. 13. The DID result even with a reference compass is worse than the moment model by landmark rearragement for no reference compass. It implies that the performance is not simply related with
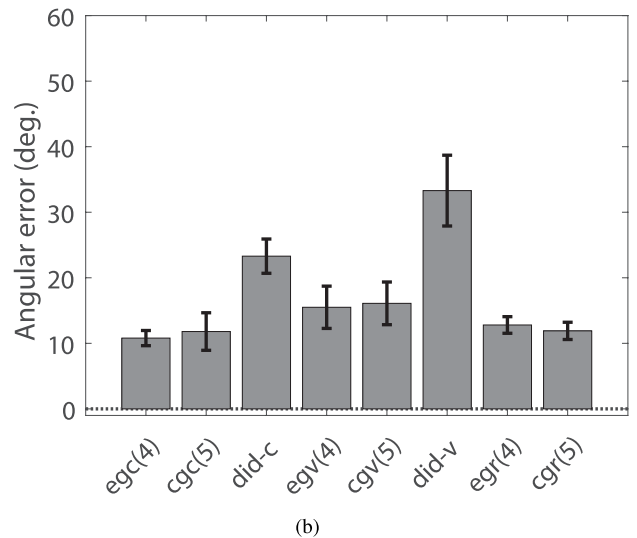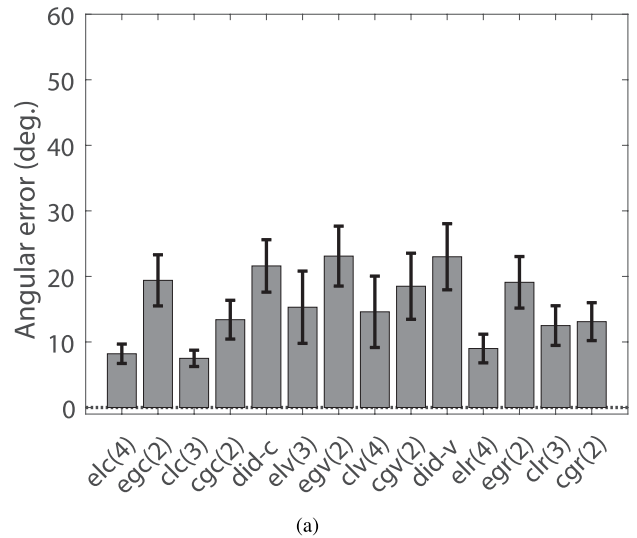

FIGURE 14. Homing performance with various methods (described in Table 1) (a) environment 'ourlab' (b) environment 'a1original' from Vardy's dataset.

whether a reference compass is available, but the performance rather depends on how to measure the landmark distribution with the landmark distance and the feature.

D. COMPARISON OF HOMING PERFORMANCES WITH VARIOUS METHODS

The homing performances with various moment models are shown in Fig. 14; more detailed results are given in Table 2-3. We tested a combination of alignment methods (with a reference compass, visual compass or landmark rearrangement), landmark features (equal intensity or color intensity), and range information (with laser sensor readings, ground-line distance estimation or image distance in the DID). As shown in Fig. 14(a), the moment model with order 3, the color intensity for the feature and laser sensor readings for the distance shows the best performance in ourlab environment; also see Table 2. High performance can be expected for the moment order $n = 3$ or greater.

TABLE 2. Angular errors with various methods for ourlab environment; mean of error (μ), 95% confidence interval (σ), the ratio (percentage) of errors $\varepsilon_1 (0 \le \varepsilon_\theta < 45°)$, $\varepsilon_2 (45 \le \varepsilon_\theta < 90°)$, $\varepsilon_3 (90 \le \varepsilon_\theta < 180°)$.

class	alignment	feature	range	n	$\mu \pm \sigma$	$0 \le \varepsilon_\theta < 45°$	$45 \le \varepsilon_\theta < 90°$	$90 \le \varepsilon_\theta < 180°$
elc(2)			laser sensor	2	10.4 ± 2.1	100	0	0
elc(3)			laser sensor	3	8.5 ± 1.5	100	0	0
elc(4)		equal intensity		4	8.2 ± 1.5	100	0	0
egc(2)			ground line	2	19.4 ± 3.9	97.1	2.9	0
egc(3)			ground line	3	24.2 ± 5.2	97.1	2.9	0
egc(4)	with			4	28.3 ± 6.3	91.2	8.8	0
clc(1)	reference		laser sensor	1	14.8 ± 5.2	89.8	8.8	1.4
clc(2)	compass		laser sensor	2	9.4 ± 1.9	100	0	0
clc(3)			laser sensor	3	7.7 ± 1.2	100	0	0
clc(4)		color		4	7.8 ± 1.2	100	0	0
cgc(2)		intensity		2	13.4 ± 3.0	100	0	0
cgc(3)			ground line	3	17.5 ± 3.8	100	0	0
cgc(4)				4	21.9 ± 4.6	100	0	0
did-c			image distance	-	21.6 ± 4.0	97.1	2.9	0
elv(2)			laser sensor	2	16.2 ± 5.8	94.1	5.9	0
elv(3)			laser sensor	3	15.3± 5.5	94.1	5.9	0
elv(4)		equal intensity		4	15.4 ± 5.4	94.1	5.9	0
egv(2)			ground line	2	23.1 ± 4.6	86.4	13.6	0
egv(3)			ground line	3	26.9 ± 5.2	88.2	11.8	0
egv(4)	visual			4	30.8 ± 6.0	85.3	14.7	0
clv(2)	compass		laser sensor	2	17.6 ± 6.3	94.1	5.9	0
clv(3)			laser sensor	3	15.4 ± 5.7	94.1	5.9	0
clv(4)		color		4	14.6 ± 5.4	94.1	5.9	0
cgv(2)		intensity		2	18.5 ± 5.0	94.1	5.9	0
cgv(3)			ground line	3	21.6 ± 4.8	94.1	5.9	0
cgv(4)				4	25.5 ± 5.2	88.2	11.8	0
did-v			image distance	-	23.0 ± 5.0	94.1	5.9	0
elr(2)			laser sensor	2	20.1 ± 5.6	94.1	5.9	0
elr(3)			laser sensor	3	12.1 ± 2.8	100	0	0
elr(4)		equal intensity		4	9.0 ± 2.2	100	0	0
egr(2)			ground line	2	19.1 ± 3.9	97.1	2.9	0
egr(3)			ground line	3	23.9 ± 5.2	94.1	5.9	0
egr(4)	rearranged			4	28.0 ± 6.3	91.2	8.8	0
clr(2)	landmarks		laser sensor	2	18.1 ± 5.4	91.2	8.8	0
clr(3)			laser sensor	3	12.5 ± 3.0	100	0	0
clr(4)		color		4	13.1 ± 2.5	100	0	0
cgr(2)		intensity		2	13.1 ± 2.9	100	0	0
cgr(3)			ground line	3	17.2 ± 3.7	100	0	0
cgr(4)				4	21.6 ± 4.5	91.2	8.8	0
cec	compass	color intensity	$r_i = 1$	-	47.2 ± 17.6	43.2	26.3	30.5

Even without laser sensor readings, the homing performance can be improved by ground-line distance estimation only with visual camera. The moment potential method outperforms the DID method with simple comparison of snapshots. As shown in Table 2, distance measure with a range sensor enhances the homing performance, compared to the estimation with ground-line distance. Real measurement of landmark distances greatly help model the landmark distribution with the moment function, although even a rough guess of landmark distances can contribute to the performance. We can consider a metric with only color features but no distance information (which is represented as a class 'cec' in Table 2-3). The homing performance is significantly worse than the moment models with distance estimation. It implies that the landmark vector approach only with visual sensor has its limitation.

E. NOISE TEST WITH THE MOMENT MODEL

The moment model assumes that the environment is isotropic; all the landmarks are observed at any point. In reality, non-isotropic conditions are prevalent. Various methods based on the moment model shown above were tested in real situations. Even with non-isotropic situations, the moment model shows reasonable homing performance. When many common parts between a pair of snapshots at two positions are available and some landmarks are missing in one snapshot, the model has an integrative property of landmark characteristics (as a sum of landmark features) and compensates for the missing or occluded landmarks. With the model, effective homing vectors are estimated because the reference point for each snapshot is not severely changed even with occluded landmarks.

In fact, landmark sizes or positions are distorted, depending on an observer's viewpoint even in the same environment, or some landmarks can be occluded. To see the robustness or limitation of the moment model, varying levels of occlusions were tested by applying salt and pepper noise on visual images. Instead of testing all the methods, we tested three representative approaches, *clc*(3), *cgc*(2) and *cgc*(5), showing robust performance in the above experiments. The method *clc*(3) uses distance information from laser sensor and visual information together; here, we keep laser sensor

TABLE 3. Angular errors with various methods for Vardy's environment; mean of error (μ), 95% confidence interval (σ), the ratio (percentage) of errors ε_1 ($0 \leq \varepsilon_\theta < 45°$), ε_2 ($45 \leq \varepsilon_\theta < 90°$), ε_3 ($90 \leq \varepsilon_\theta < 180°$).

class	alignment	feature	range	n	$\mu \pm \sigma$	$0 \leq \varepsilon_\theta < 45°$	$45 \leq \varepsilon_\theta < 90°$	$90 \leq \varepsilon_\theta < 180°$
egc(2)		equal intensity		2	17.0 ± 1.4	100	0	0
egc(3)		equal intensity		3	12.7 ± 1.2	100	0	0
egc(4)				4	10.8 ± 1.1	100	0	0
cgc(1)	reference compass	color intensity	ground line	1	33.3 ± 4.2	72.2	24.3	3.5
cgc(2)				2	20.7 ± 1.9	97.1	2.9	0
cgc(3)				3	16.5 ± 1.6	99.4	0.6	0
cgc(4)				4	12.8 ± 1.4	100	0	0
cgc(5)				5	11.8 ± 1.3	100	0	0
did-c		image dist.	-		23.3 ± 2.5	97.1	2.9	0
egv(2)		equal intensity		2	21.4 ± 3.1	95.9	0.6	3.5
egv(3)		equal intensity		3	17.4 ± 3.1	95.9	0.6	3.5
egv(4)				4	15.5 ± 3.1	95.9	0.6	3.5
cgv(2)	visual compass	color intensity	ground line	2	27.0 ± 3.1	88.8	8.3	2.9
cgv(3)				3	18.1 ± 3.2	96.5	0	3.5
cgv(4)				4	17.6 ± 3.1	96.5	0	3.5
cgv(5)				5	16.1 ± 3.1	96.5	0	3.5
did-v		image dist.	-		33.3 ± 5.2	79.9	11.8	8.3
egr(2)		equal intensity		2	22.7 ± 1.8	95.3	4.7	0
egr(3)		equal intensity		3	17.0 ± 1.5	100	0	0
egr(4)				4	12.8 ± 1.2	100	0	0
cgr(2)	landmark rearrangement	color intensity	ground line	2	20.7 ± 2.0	97.1	2.9	0
cgr(3)				3	16.5 ± 1.6	99.4	0.6	0
cgr(4)				4	13.0 ± 1.4	100	0	0
cgr(5)				5	11.9 ± 1.3	100	0	0
cec	compass	color intensity	$r_i = 1$	-	43.9 ± 6.3	47.1	17.5	35.4

information without adding the artificial noise, but noise is added only to visual images. The methods $cgc(2)$ and $cgc(5)$ extract distance and color information from visual image, and both are affected by artificial noise. Table 4 shows angular errors for homing depending on artificial occlusion rate (noise rate). A high rate of salt-pepper noise affects the homing performance, but under a noise rate of 30%, reasonable homing results are observed. It indicates many common landmarks or similar landscape tones available helps guide homing. Especially, $cgc(2)$ and $cgc(5)$ has distance estimation with ground-line of the visual image. More distance errors are expected with higher noise rate. In short, we argue that our model can be operated in the environments with partial occlusions or noisy sensor readings, and errors in distance measurement have larger effect on homing performance than those in visual information.

IV. DISCUSSION

In this paper, we suggest a new navigation method based on high-order moment measure using two types of sensor readings, laser sensor and visual sensor. The moment function characterizes the landmark distribution with the landmark feature, and interestingly, it builds a potential measure with the unique mimimum point. The moment potential has a convex property when the moment order is greater than or equal to one. It allows to use that point as a reference point, regardless of any current view. If the order is negative, it forms a local potential around each landmark object. The property can be used as obstalce avoidance; high potential field indicates close to any obstacle for negative moment order.

The moment models depend on whether a reference compass is available, whether the color intensity is used as

TABLE 4. Angular errors with salt and pepper noise; selected methods $clc(3)$ and $cgc(2)$ were tested with 'ourlab' environment and $cgc(5)$ was tested with Vardy's environment (first column indicates the noise percentage on the visual images, and each case shows the performance $\mu \pm \sigma$ with the averaged angular error (deg.) and 95% confidence interval (σ)).

noise rate	clc(3)	cgc(2)	cgc(5)
0%	7.7 ± 1.2	13.4 ± 3.0	11.8 ± 1.3
10%	8.8 ± 1.6	26.3 ± 15.6	12.8 ± 2.4
20%	9.4 ± 1.4	36.5 ± 12.2	13.3 ± 2.4
30%	14.9 ± 1.4	73.6 ± 18.5	22.8 ± 4.4
40%	10.3 ± 1.8	49.9 ± 14.2	42.7 ± 3.7
50%	17.5 ± 2.8	75.6 ± 18.7	45.3 ± 6.3
60%	16.8 ± 3.0	67.0 ± 17.0	39.8 ± 6.6
70%	20.0 ± 4.3	81.8 ± 18.6	49.4 ± 6.7
80%	22.0 ± 4.3	46.3 ± 16.6	55.0 ± 7.8

a feature or no feature is used, or whether the distance estimation in the image is applied. In many cases, high-order moment functions are useful, generally the order $n = 3$ or $n = 4$ is effective to find the homing direction accurately. Our previous work only focused on the moment order $n = 2$ but the performance can be further improved with higher order. Another variation with the moment function is possible; the area integration over the inner side of landmarks. We showed that our formulation with the area integration is equivalent to the integration on the landmark position line, but only differ in the order (increasing the order by 2). That shows that higher-order moment potentials are useful in the analysis of the landmark distribution.

In this paper, we did not take any object-feature extraction process, but instead a holistic view about landmarks was considered. The whole pixels were regarded as a collection of landmarks. If the object-feature extraction is applied, by separating objects from the background, a discretized set of
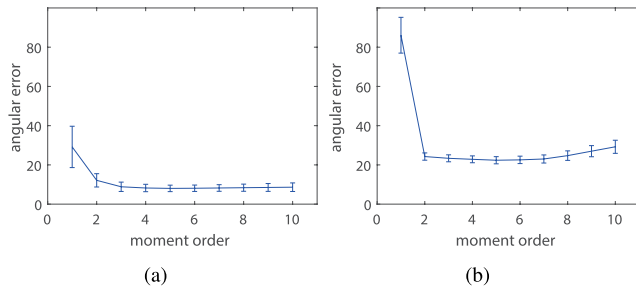
FIGURE 15. Homing performances with varying moment orders by the numerical search for a reference point (with color intensity for the feature) (a) 'outlab' environment (with laser sensor readings for distance) (b) Vardy's environment (with ground-line distance estimation).

landmarks can be obtained. The moment models over this set may be an alternative approach.

In our experiments, varying moment orders were investigated. Generally, the order $n = 3$ or $n = 4$ showed the best average performance in angular errors for homing. The best order can also depend on how to describe the landmark distribution, for example, the area integration in space or the position integration for objects. More complex type of description about the environment seems to need high-order potentials. The moment concept is used in physics or mathematics for the shape of a collection of points, and the moment has different meanings relying on the order. In mathematics, the first moment is the mean, the second moment is the variance, the third is the skewness, and the fourth is the kurtosis.

We may extend the current moment model into a complex model with alignment methods. For instance, as an extension of the moment function, we can build the moment inertia matrix forming the inertia tensor set. We can estimate the rotational component for alignment of two snapshots by comparing two moment inertia matrices at two different locations. This could be an alternative method for alignment.

The suggested moment model assumes the environment is isotropic, that is, the landmark distribution keeps the same at any observing position. In real world, that assumption is not always true and many occlusions of landmarks occur or the object sizes change depending on the view location. In robotic experiments, measurement errors can be observed in visual sensor and range sensor. More noise errors are prevalent in the visual snapshot. For example, various illumination effect in pictures can occur depending on the light source and its position or glittering of the floor. It greatly influences homing performance. Yet the experiments showed that our approach guides well homing directions at test positions, regardless of those environmental conditions.

We mentioned that there is an iterative approach to find the convergence point more exactly in equation (6), but it needs more computing time. Another simple estimation of homing vector is available in equation (9). In experiments we used the second method based on the gradient-descent approach to reduce the computing time. We investigated how the homing performance is influenced by more accurate estimation of the reference point (convergence point with the minimum moment potential). If the reference point is accurately

estimated by the numerical search, almost the same homing performance is observed, regardless of the moment order greater than $n = 3$ or 4 – see Fig. 15, while the gradient-descent method leads to a rough estimation of homing vector for high-order moment functions. That is, accurate estimation of the reference point improves the homing performance.

As mentioned above, the moment model with ground-line distance estimation is worse in homing performance than that with direct distance measurement with laser sensor readings. Conversion from the ground line in the omnidirectional camera image to the distance may include distance errors, when the mirror structure in the omnidirectional camera or calibration information is not given, as often experienced in Vardy's environment. In that case, it may be involved with misleading estimation of landmark distribution, causing relatively large homing errors, even though the numerical search for a reference point is applied.

Our moment model follows the bio-inspired snapshot model suggested by Cartwright and Collett [26]. That is, the model determines homing directions by comparing the snapshot taken at an arbitrary spot and the home snapshot. Unlike other bio-inspired navigation approaches, the model characterizes the environmental landscape with moment features consisting of distance and color information, while other snapshot-based approaches generally use individual landmark features from visual image. The high-order moments outline the snapshot as a holistic view rather than extract landmark features. It is an open question if the moment features can also be found in the animal navigation system, although it could be a plausible hypothesis. At least the moment function suggests an effective union of distance and visual feature such as color intensity. The method need not any clustering of image intensity, matching process of features, or map building process that many navigation systems often use. The property itself is a good advantage in the local navigation system. The approach outperforms the DID (Descent in Image Distance) method [34] which is a state-of-art holistic approach in local homing navigation with visual image. The moment model effectively uses the environmental characteristics for landmark distribution. As shown in Table 2-3, the suggested model with higher orders is mostly significantly better than a simple model with second-order moments [56].

V. CONCLUSION

In this paper, we suggest high-order moment models to handle local homing navigation with a range sensor and visual camera. The moment model originates from the physical model of inertia of moment to handle the mass distribution. A general form of moment model with varying orders is provided to represent the landmark distribution. Local homing navigation is largely influenced by the landmark distribution and features. We analyzed the effect of moment orders on local homing navigation. The suggested approach used a holistic view on the landmarks in the panoramic snapshot without any landmark object extraction, where it is assumed that the whole pixels

in the omnidirectional snapshot represent a collection of landmarks.

The snapshot model suggested by Cartwright and Collett [26] was applied to the moment models here, and two snapshots including the range sensor and the image observed at two different locations, the target position and the current location, are compared to determine the direction to the target position. The moment model shows how to combine the two different sensor modalities effectively in a simple form.

In this paper, we suggest that local homing navigation with high-order moments is successful to reach the goal, starting at any position, when it is assumed that the moment measure holds constant or similar from any view. We provide a convergence proof that for any moment order ($n \geq 1$), the moment potential has the unique minimum potential and the homing vector can be converged into the home location. Interestingly, even in the real environments with noisy sensor readings, or partial occlusions, homing directions are effectively estimated. We demonstrated various condition tests to estimate homing vectors at many grid positions. High-order moment potential function with $n = 3, 4$ or 5 can derive the best average homing performance depending on the environment. This work shows a potential of any link between position information and feature information in pixel level or in landmark object scale which can be applied to various application areas with the moment concept.

The current work suggests that a mobile robot can return home in real environments, if it has a range sensor and visual sensor together. Our experimental results support that the landmark distance measured with a range sensor is a cruicial factor for local homing navigation, since it can estimate the landmark distribution more accurately. Only with visual sensor, the landmark distance can be estimated with ground-line distance in the indoor environment with floor. The approach may have a limitation in cluttered environments with difficluty in estimating the ground line of objects. We need further study to develop homing navigation only with the omnidirectional snapshots or find its limitation, and to characterize objects in visual image as a set of features.

For the future work, we can extend our model into the long-ranged homing with many occlusions of landmarks. The moment model is designed for local homing, but it can be applied to long-ranged homing with a set of reference snapshots. We can place several milestone positions in an exploration path as local home positions, and a series of local homing can handle long-ranged homing. With this place cell approach, the suggested model can also be used for homing in the environment with many varieties of landscapes.

APPENDIX
PROOF OF THE CONVEX PROPERTY IN HIGH-ORDER MOMENT MODEL

The moment function with order n is given by

$$M_n = \sum_{i=1}^{N} r_i^n C_i = \sum_{i=1}^{N} ((a_i - x)^2 + (b_i - y)^2)^{\frac{n}{2}} C_i \quad (14)$$

where there are N landmarks measured in the omnidirectional space, r_i is the range value for the i-th landmark, which is the distance to the i-th feature, C_i. Its location is (a_i, b_i) in the relative coordinate from an observing point. The relative distance from an arbitrary position (x, y) to (a_i, b_i) can be calculated.

Then we take the gradient of the moment function as follows:

$$\nabla M_n = \sum_{i=1}^{N} nr_i^{n-2}[(x - a_i)C_i, \quad (y - b_i)C_i] \quad (15)$$

where this gradient vector is the slope of the moment potential at a position (x, y).

To find the minimum convergence point in the convex function, we need to calculate the determinant of Hessian matrix

$$\mathbf{H} = \begin{pmatrix} \dfrac{d^2 M_n}{dx^2} & \dfrac{d^2 M_n}{dxdy} \\ \dfrac{d^2 M_n}{dxdy} & \dfrac{d^2 M_n}{dy^2} \end{pmatrix} = \begin{bmatrix} M_{n,xx} & M_{n,xy} \\ M_{n,yx} & M_{n,yy} \end{bmatrix} \quad (16)$$

where $M_{n,xx}$, $M_{n,xy}$ and $M_{n,yy}$ are second-order differential terms. That is, the matrix consists of second-order partial derivatives of the moment function.

The conditions for the unique convergence point are given by

$$\det(\mathbf{H}) > 0, \quad M_{n,xx} > 0, \quad (17)$$

which are related to the convex property of the moment function with the unique global convergence.

Then the Hessian matrix is calculated as

$$\mathbf{H} = \sum_{i=1}^{N} \beta_i \begin{bmatrix} (n-1)X_i^2 + Y_i^2 & (n-2)X_iY_i \\ (n-2)X_iY_i & X_i^2 + (n-1)Y_i^2 \end{bmatrix}$$

where $X_i = (a_i - x)$, $Y_i = (b_i - y)$ and $\beta_i = nC_i\{(a_i - x)^2 + (b_i - y)^2\}^{n/2-2}$.

We see that $M_{n,xx}$ and $M_{n,yy}$ are positive with $n \geq 1$. The determinant of the Hessian matrix is given by

$$\det(\mathbf{H}) = \sum_{i=1}^{N} \beta_i\{(n-1)X_i^2 + Y_i^2\} \sum_{j=1}^{N} \beta_j\{X_j^2 + (n-1)Y_j^2\}$$

$$- \sum_{i=1}^{N} \beta_i\{(n-2)X_iY_i\} \sum_{j=1}^{N} \beta_j\{(n-2)X_jY_j\} \quad (18)$$

Then the above equation can be re-written into two terms (term for $i = j$ and term $\mathbf{R}$ for $i \neq j$) as follows:

$$\det(\mathbf{H}) = \sum_{i=1}^{N} [\beta_i^2(n-1)(X_i^2 + Y_i^2)^2] + \mathbf{R}$$

$$= \sum_{i=1}^{N} n^2(n-1)(r_i^n C_i)^2/r_i^4 + \mathbf{R} \quad (19)$$

where $r_i = (X_i^2 + Y_i^2)^{1/2}$. The term $\mathbf{R}$ can be calculated as follows:

$$\mathbf{R} = \sum_{i=1}^{n-1} \sum_{j=i+1}^{n} \beta_i \beta_j \begin{pmatrix} (n-1)X_i^2 X_j^2 + (n-1)^2 X_i^2 Y_j^2 \\ +X_j^2 Y_i^2 + (n-1)Y_i^2 Y_j^2 \\ +(n-1)X_j^2 X_i^2 + (n-1)^2 X_j^2 Y_i^2 \\ +X_i^2 Y_j^2 + (n-1)Y_j^2 Y_i^2 \\ -2(n-2)^2 X_i X_j Y_i Y_j \end{pmatrix}$$

$$= \sum_{i=1}^{n-1} \sum_{j=i+1}^{n} \beta_i \beta_j [(n^2 - 2n + 2)(X_i Y_j - X_j Y_i)^2 + 2(n-1)(X_i X_j + Y_i Y_j)^2]$$

$$= \sum_{i=1}^{n-1} \sum_{j=i+1}^{n} \beta_i \beta_j [\{(n-1)^2 + 1\}(X_i Y_j - X_j Y_i)^2 + 2(n-1)(X_i X_j + Y_i Y_j)^2] \quad (20)$$

Thus, the determinant of the Hessian matrix is

$$\det(\mathbf{H}) = \sum_{i=1}^{N} n^2(n-1)(r_i^n C_i)^2 / r_i^4$$
$$+ \sum_{i=1}^{n-1} \sum_{j=i+1}^{n} \beta_i \beta_j [\{(n-1)^2 + 1\}(X_i Y_j - X_j Y_i)^2 + 2(n-1)(X_i X_j + Y_i Y_j)^2] \quad (21)$$

Hence, $n \geq 1$ is a sufficient condition to obtain the unique global convergence point for the moment function. For $n \leq 0$, it has no convergence point. The condition $0 < n < 1$ cannot tell us whether there is a unique convergence point.

REFERENCES

[1] A. Widyotriatmo and K.-S. Hong, "Navigation function-based control of multiple wheeled vehicles," *IEEE Trans. Ind. Electron.*, vol. 58, no. 5, pp. 1896–1906, May 2011.

[2] B. Zhu, A. H. B. Zaini, and L. Xie, "Distributed guidance for interception by using multiple rotary-wing unmanned aerial vehicles," *IEEE Trans. Ind. Electron.*, vol. 64, no. 7, pp. 5648–5656, Jul. 2017.

[3] T. Zhang, S. Huang, D. Liu, L. Shi, C. Zhou, and R. Xiong, "A method of state estimation for underwater vehicle navigation around a cylindrical structure," in *Proc. IEEE 11th Conf. Ind. Electron. Appl. (ICIEA)*, Jun. 2016, pp. 101–106.

[4] X. Huang and Y. Yan, "Output feedback control of underactuated spacecraft hovering in circular orbit with radial or in-track controller failure," *IEEE Trans. Ind. Electron.*, vol. 63, no. 9, pp. 5569–5581, Sep. 2016.

[5] A. Gilg and G. Schmidt, "Landmark-oriented visual navigation of a mobile robot," *IEEE Trans. Ind. Electron.*, vol. 41, no. 4, pp. 392–397, Aug. 1994.

[6] W. Wang and G. Xie, "Online high-precision probabilistic localization of robotic fish using visual and inertial cues," *IEEE Trans. Ind. Electron.*, vol. 62, no. 2, pp. 1113–1124, Feb. 2015.

[7] S. Park and S. Hashimoto, "Autonomous mobile robot navigation using passive RFID in indoor environment," *IEEE Trans. Ind. Electron.*, vol. 56, no. 7, pp. 2366–2373, Jul. 2009.

[8] S. E. Lyshevski, "Signal processing in cyber-physical MEMS sensors: Inertial measurement and navigation systems," *IEEE Trans. Ind. Electron.*, vol. 64, no. 12, pp. 9618–9625, Dec. 2017.

[9] F. J. Delgado, J. M. Quero, J. Garcia, C. L. Tarrida, P. R. Ortega, and S. Bermejo, "Accurate and wide-field-of-view MEMS-based sun sensor for industrial applications," *IEEE Trans. Ind. Electron.*, vol. 59, no. 12, pp. 4871–4880, Dec. 2012.

[10] C. Darwin, "Origin of certain instincts," *Nature*, vol. 7, pp. 417–418, Apr. 1873.

[11] T. Kimchi, A. S. Etienne, and J. Terkel, "A subterranean mammal uses the magnetic compass for path integration," *Proc. Nat. Acad. Sci. USA*, vol. 101, no. 4, pp. 1105–1109, 2004.

[12] R. J. Vickerstaff and T. Merkle, "Path integration mediated systematic search: A Bayesian model," *J. Theor. Biol.*, vol. 307, pp. 1–19, Aug. 2012.

[13] S. Wintergerst and B. Ronacher, "Discrimination of inclined path segments by the desert ant *Cataglyphis fortis*," *J. Comparative Physiol. A, Neuroethol., Sensory, Neural, Behav. Physiol.*, vol. 198, no. 5, pp. 363–373, 2012.

[14] R. Wehner, "Early ant trajectories: Spatial behaviour before behaviourism," *J. Comparative Physiol. A*, vol. 202, no. 4, pp. 247–266, 2016.

[15] S. F. Reid, A. Narendra, J. M. Hemmi, and J. Zeil, "Polarised skylight and the landmark panorama provide night-active bull ants with compass information during route following," *J. Exp. Biol.*, vol. 214, no. 3, pp. 363–370, 2011.

[16] K. Basten and H. A. Mallot, "Simulated visual homing in desert ant natural environments: Efficiency of skyline cues," *Biol. Cybern.*, vol. 102, no. 5, pp. 413–425, 2010.

[17] A. Wystrach, G. Beugnon, and K. Cheng, "Ants might use different view-matching strategies on and off the route," *J. Exp. Biol.*, vol. 215, no. 1, pp. 44–55, 2012.

[18] A. Garm, M. Oskarsson, and D.-E. Nilsson, "Box jellyfish use terrestrial visual cues for navigation," *Current Biol.*, vol. 21, no. 9, pp. 798–803, 2011.

[19] J. Zeil and J. M. Hemmi, "The visual ecology of fiddler crabs," *J. Comparative Physiol. A*, vol. 192, no. 1, pp. 1–25, 2006.

[20] A. Garm and D.-E. Nilsson, "Visual navigation in starfish: First evidence for the use of vision and eyes in starfish," *Proc. Roy. Soc. B, Biol. Sci.*, vol. 281, no. 1777, p. 20133011, 2014.

[21] A. Ugolini, G. Borgioli, G. Galanti, L. Mercatelli, and T. Hariyama, "Photoresponses of the compound eye of the sandhopper *Talitrus saltator* (Crustacea, Amphipoda) in the ultraviolet-blue range," *Biol. Bull.*, vol. 219, no. 1, pp. 72–79, 2010.

[22] K. Steck, M. Knaden, and B. S. Hansson, "Do desert ants smell the scenery in stereo?" *Animal Behav.*, vol. 79, no. 4, pp. 939–945, 2010.

[23] J. L. Gould, "Animal navigation: Birds have magnetic maps," *Current Biol.*, vol. 25, no. 19, pp. R836–R838, 2015.

[24] T. S. Collett and P. Graham, "Insect navigation: Do honeybees learn to follow highways?" *Current Biol.*, vol. 25, no. 6, pp. R240–R242, 2015.

[25] T. S. Collett, A. Wystrach, and P. Graham, "Insect orientation: The travails of going straight," *Current Biol.*, vol. 26, no. 11, pp. R461–R463, 2016.

[26] B. Cartwright and T. Collett, "Landmark learning in bees," *J. Comparative Physiol.*, vol. 151, no. 4, pp. 521–543, 1983.

[27] D. Lambrinos, R. Moller, T. Labhart, R. Pfeifer, and R. Wehner, "A mobile robot employing insect strategies for navigation," *Robot. Auto. Syst.*, vol. 30, pp. 39–64, Jan. 2000.

[28] S.-E. Yu and D. Kim, "Landmark vectors with quantized distance information for homing navigation," *Adapt. Behav.*, vol. 19, no. 2, pp. 121–141, 2011.

[29] S.-E. Yu, C. Lee, and D. Kim, "Analyzing the effect of landmark vectors in homing navigation," *Adapt. Behav.*, vol. 20, no. 5, pp. 337–359, 2012.

[30] M. Liu, C. Pradalier, and R. Siegwart, "Visual homing from scale with an uncalibrated omnidirectional camera," *IEEE Trans. Robot.*, vol. 29, no. 6, pp. 1353–1365, Dec. 2013.

[31] M. Gupta, G. K. Arunkumar, and L. Vachhani, "Bearing only visual homing: Observer based approach," in *Proc. 25th Medit. Conf. IEEE Control Autom. (MED)*, Jul. 2017, pp. 358–363.

[32] R. Strydom, A. Denuelle, and M. V. Srinivasan, "Bio-inspired principles applied to the guidance, navigation and control of UAS," *Aerospace*, vol. 3, no. 3, p. 21, 2016.

[33] A. A. Argyros, K. E. Bekris, S. C. Orphanoudakis, and L. E. Kavraki, "Robot homing by exploiting panoramic vision," *Auto. Robots*, vol. 19, no. 1, pp. 7–25, 2005.

[34] J. Zeil, M. I. Hofmann, and J. S. Chahl, "Catchment areas of panoramic snapshots in outdoor scenes," *J. Opt. Soc. Amer. A, Opt. Image Sci.*, vol. 20, no. 3, pp. 450–469, 2003.

[35] R. Möller, A. Vardy, S. Kreft, and S. Ruwisch, "Visual homing in environments with anisotropic landmark distribution," *Auto. Robots*, vol. 23, no. 3, pp. 231–245, 2007.

[36] A. Vardy, "Long-range visual homing," in *Proc. IEEE Int. Conf. Robot. Biomimetics (ROBIO)*, Dec. 2006, pp. 220–226.

[37] A. Denuelle, S. Thurrowgood, F. Kendoul, and M. V. Srinivasan, "A view-based method for local homing of unmanned rotorcraft," in *Proc. 6th Int. Conf. IEEE Autom., Robot. Appl. (ICARA)*, Feb. 2015, pp. 443–449.

[38] A. Denuelle, R. Strydom, and M. V. Srinivasan, "Snapshot-based control of UAS hover in outdoor environments," in *Proc. IEEE Int. Conf. Robot. Biomimetics (ROBIO)*, Dec. 2015, pp. 1278–1284.

[39] D. Churchill and A. Vardy, "Homing in scale space," in *Proc. IEEE/RSJ Int. Conf. Intell. Robots Syst.*, Sep. 2008, pp. 1307–1312.

[40] D. Churchill and A. Vardy, "An orientation invariant visual homing algorithm," *J. Intell. Robot. Syst.*, vol. 71, no. 1, pp. 3–29, 2013.

[41] M. O. Franz, B. Schölkopf, H. A. Mallot, and H. H. Bülthoff, "Where did I take that snapshot? Scene-based homing by image matching," *Biol. Cybern.*, vol. 79, no. 3, pp. 191–202, 1998.

[42] M. Franz, "Minimalistic visual navigation=, Minimalistische visuelle Navigation," Ph.D. dissertation, Univ. Tübingen, Tübingen, Germany, 1999.

[43] J. Hong, X. Tan, B. Pinette, R. Weiss, and E. M. Riseman, "Image-based homing," *IEEE Control Syst. Mag.*, vol. 12, no. 1, pp. 38–45, Feb. 1992.

[44] R. Möller, M. Krzykawski, and L. Gerstmayr, "Three 2D-warping schemes for visual robot navigation," *Auto. Robots*, vol. 29, nos. 3–4, pp. 253–291, 2010.

[45] F. Labrosse, "Short and long-range visual navigation using warped panoramic images," *Robot. Auto. Syst.*, vol. 55, no. 9, pp. 675–684, 2007.

[46] W. Stürzl and R. Möller, "An insect-inspired active vision approach for orientation estimation with panoramic images," in *Bio-inspired Modeling of Cognitive Tasks. IWINAC* (Lecture Notes in Computer Science), vol. 4527, J. Mira and J. R. Álvarez, Eds. Berlin, Germany: Springer, 2007, pp. 61–70.

[47] R. Möller, "A model of ant navigation based on visual prediction," *J. Theor. Biol.*, vol. 305, pp. 118–130, Jul. 2012.

[48] R. Möller, "A SIMD implementation of the MinWarping method for local visual homing," Fac. Technol., Comput. Eng., Bielefeld Univ., Bielefeld, Germany, Tech. Rep., 2016.

[49] R. Möller, "Column distance measures and their effect on illumination tolerance in MinWarping," Fac. Technol., Comput. Eng. Group, Univ. Bielefeld, Bielefeld, Germany, Tech. Rep., 2016

[50] D. Fleer and R. Möller, "Comparing holistic and feature-based visual methods for estimating the relative pose of mobile robots," *Robot. Auto. Syst.*, vol. 89, pp. 51–74, Mar. 2017.

[51] Q. Zhu, C. Liu, and C. Cai, "A novel robot visual homing method based on SIFT features," *Sensors*, vol. 15, no. 10, pp. 26063–26084, 2015.

[52] A. Vardy and R. Möller, "Biologically plausible visual homing methods based on optical flow techniques," *Connection Sci.*, vol. 17, nos. 1–2, pp. 47–89, 2005.

[53] R. Möller, M. Horst, and D. Fleer, "Illumination tolerance for visual navigation with the holistic min-warping method," *Robotics*, vol. 3, no. 1, pp. 22–67, 2014.

[54] C. Lee, S. E. Yu, and D. Kim, "Landmark-based homing navigation using omnidirectional depth information," *Sensors*, vol. 17, no. 8, p. 1928, 2017.

[55] T.-B. Kwon and J.-B. Song, "A new feature commonly observed from air and ground for outdoor localization with elevation map built by aerial mapping system," *J. Field Robot.*, vol. 28, no. 2, pp. 227–240, 2011.

[56] C. Lee and D. Kim, "Local homing navigation based on the moment model for landmark distribution and features," *Sensors*, vol. 17, no. 11, p. 2658, 2017.

[57] S.-E. Yu and D. Kim, "Image-based homing navigation with landmark arrangement matching," *Inf. Sci.*, vol. 181, no. 16, pp. 3427–3442, 2011.

CHANGMIN LEE received the B.E. degree from the Department of Electrical and Electronic Engineering, Yonsei University, South Korea, and the Ph.D. degree from Yonsei University in 2018. His research interests are in the areas of visual navigation, artificial intelligence, and neural networks.
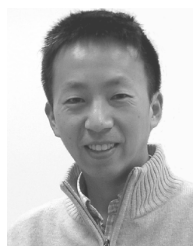
DAEEUN KIM received the B.E. and M.S. degrees from the Department of Computer Science and Engineering, Seoul National University, and the University of Michigan, Ann Arbor, respectively, and the Ph.D. degree from The University of Edinburgh in 2002. From 2002 to 2006, he was a Research Scientist with the Max Planck Institute for Human Cognitive and Brain Sciences. He is currently an Associate Professor with Yonsei University, South Korea. His research interests are in the areas of biorobotics, autonomous robots, artificial life, neural networks, and neuroethology.

● ● ●